

1 An improved process-oriented hydro-biogeochemical model for 2 simulating dynamic fluxes of methane and nitrous oxide in alpine 3 ecosystems with seasonally frozen soils

4 Wei Zhang¹, Zhisheng Yao¹, Siqi Li¹, Xunhua Zheng^{1, 2}, Han Zhang^{1, 3}, Lei Ma^{1, 4}, Kai Wang¹, Rui
5 Wang¹, Chunyan Liu¹, Shenghui Han¹, Jia Deng⁵, Yong Li¹

6 ¹State Key Laboratory of Atmospheric Boundary Layer Physics and Atmospheric Chemistry, Institute of Atmospheric
7 Physics, Chinese Academy of Sciences, Beijing 100029, P. R. China

8 ²College of Earth and Planetary Science, University of Chinese Academy of Sciences, Beijing 100049, P. R. China

9 ³School of Geographic and Environmental Sciences, Tianjin Normal University, Tianjin 300387, P. R. China

10 ⁴Institute of Meteorology and Climate Research, Atmospheric Environmental Research (IMK-IFU), Karlsruhe Institute of
11 Technology, Kreuzackbahnstrasse 19, 82467 Garmisch-Partenkirchen, Germany

12 ⁵Complex Systems Research Center, Institute for the Study of Earth, Oceans and Space, University of New Hampshire, 39
13 College Road, Durham, NH 03824, USA

14

15 *Correspondence to:* Xunhua Zheng (xunhua.zheng@post.iap.ac.cn)

16 **Abstract.** The hydro-biogeochemical model Catchment Nutrient Management Model - DeNitrification-DeComposition
17 (CNMM-DNDC) was established to simultaneously quantify ecosystem productivity and losses of nitrogen and carbon at the
18 site or catchment scale. As a process-oriented model, this model is expected to be universally applied to different climate
19 zones, soils, land uses and field management practices. This study is one of many efforts to fulfil such an expectation, which
20 was performed to improve the CNMM-DNDC by incorporating a physical-based soil thermal module to simulate the soil
21 thermal regime in the presence of freeze-thaw cycles. The modified model was validated with simultaneous field
22 observations in three typical alpine ecosystems (wetlands, meadows and forests) within a catchment located in the seasonally
23 frozen region of the eastern Tibetan Plateau, including soil profile temperature, topsoil moisture and fluxes of methane (CH₄)
24 and nitrous oxide (N₂O). The validation showed that the modified CNMM-DNDC was able to simulate the observed
25 seasonal dynamics and magnitudes of above variables in the three typical alpine ecosystems, with index of agreement values
26 of 0.91–1.00, 0.49–0.83, 0.57–0.88 and 0.26–0.47, respectively. Consistent with the emissions determined from the field
27 observations, the simulated aggregate emissions of CH₄ and N₂O were highest for the wetland among three alpine
28 ecosystems, which were dominated by the CH₄ emissions. This study indicates the possibility for utilizing the process-
29 oriented model CNMM-DNDC to predict hydro-biogeochemical processes, as well as related gas emissions, in seasonally
30 frozen regions. As the original CNMM-DNDC was previously validated in some unfrozen regions, the modified CNMM-
31 DNDC could be potentially applied to estimate the emissions of CH₄ and N₂O from various ecosystems under different
32 climate zones at the site or catchment scale.

33 **1 Introduction**

34 During the last 50 years, the extraordinary changes in the nitrogen and carbon cycles have occurred globally, which are
35 essential components of ecosystems (e.g., Galloway *et al.*, 2008; Canfield *et al.*, 2010). Climate changes due to warming and
36 human anthropogenic activities derived from food production have significantly altered the cycling of nitrogen and carbon
37 and led to increased reactive nitrogen availability and carbon losses, which result in a series of environmental problems at
38 the catchment, regional and even global scales (e.g., Galloway *et al.*, 2004; Galloway *et al.*, 2008; Ju *et al.*, 2009). Excessive
39 reactive nitrogen in soils can be lost in the forms of nitrogen gases, such as nitrous oxide (N₂O), nitric oxide (NO) and
40 ammonia (NH₃), and nitrogen pollution, such as nitrate (NO₃⁻) and ammonium (NH₄⁺), in water through leaching or surface
41 runoff (e.g., Seitzinger, 2008; Collins *et al.*, 2016). In the face of increased air temperatures and intensive land use changes,
42 especially in cold regions, the soil organic carbon stored since the Last Glacial Maximum has been lost to the atmosphere via
43 methane (CH₄) and carbon dioxide (CO₂) (e.g., Piao *et al.*, 2009; Fenner and Freeman, 2011; Schuur *et al.*, 2015). These
44 nitrogen and carbon losses contribute to potential global warming (CO₂, CH₄ and N₂O), air pollution (NO and NH₃) and
45 surface/groundwater pollution (NO₃⁻ and NH₄⁺). Therefore, sustainable ecosystems urgently need to be established that not
46 only focus on net primary productivity but also are friendly to the environment with the minimal hazards, including
47 greenhouse gases, air pollution and water pollutants (e.g., Cui *et al.*, 2018; Zhang *et al.*, 2019).

48 The cycling of nitrogen and carbon is closely related to soil water processes (e.g., Breuer *et al.*, 2010; Vereecken *et al.*,
49 2016; Zhang *et al.*, 2018b). Thus, interactions among soil waters and the cycling of nitrogen and carbon govern biological
50 productivity and environmental outcomes (e.g., Zhu *et al.*, 2018). The interactions consist of the redox potential for different
51 transformation processes influenced by the spatiotemporal variation in soil water content and the lateral transport of water
52 and dissolved nitrogen or carbon controlled by surface and subsurface flow (e.g., McClain *et al.*, 2003; Castellano *et al.*,
53 2013; Bechmann, 2014). For example, the variation in soil water content can create hot spots or moments of nitrogen and
54 carbon losses by influencing plant nitrogen uptake, redox potential, and the transport of dissolved nitrogen and carbon (e.g.,
55 Zhu *et al.*, 2012; Keiluweit *et al.*, 2017). Therefore, a complete understanding of biogeochemical processes will inevitably
56 involve interactions among soil water and the cycling of nitrogen and carbon (e.g., Breuer *et al.*, 2010; Vereecken *et al.*,
57 2016; Zhu *et al.*, 2018).

58 Biogeochemical models, such as DNDC, LandscapeDNDC, WNMM, MOMOS, CENTURY and DayCent, are
59 effective tools for simulating the cycling of nitrogen and carbon and quantifying the effects of climate change and
60 anthropogenic activities on ecosystems (e.g., Foereid *et al.*, 2007; Haas *et al.*, 2012; Li, 2007; Li *et al.*, 2007; Pansu *et al.*,
61 2010; Cheng *et al.*, 2014; Pansu *et al.*, 2014). In recent years, some new conceptual approaches are applied in the
62 biogeochemical models, such as centering on the functional role of the soil microbial biomass (Pansu *et al.*, 2010; Pansu *et al.*,
63 2014) and detailing the lateral transport of water and nutrients (Haas *et al.*, 2012; Zhang *et al.*, 2018b). Generally,
64 comprehensive hydrological processes, especially for the lateral transport of water and nutrients, are simplified or ignored in
65 most models due to specific questions that must be addressed (e.g., Li, 2007; Li *et al.*, 2007; Chen *et al.*, 2008; Deng *et al.*,

66 2014). For the land surface or hydrological models at large scales, they are designed with explicit mechanisms of hydrology
67 and generally focus on vertical and lateral nutrient transport, such as nitrate loads into rivers (e.g., Liu *et al.*, 2019). However,
68 the simulations of nitrogen and carbon processes are usually based on empirical functions even without predicting gas loss.
69 Due to the various purposes of different models, coupling soil hydrological models with biogeochemical models can be an
70 effective strategy for integrating soil water and cycling of nitrogen and carbon to improve model performance. Thus, the
71 coupled model with improved performance can be applied to simultaneously predict productivity and potential negative
72 environmental effects (e.g., Chen *et al.*, 2008; Zhu *et al.*, 2018).

73 In recent years, efforts have been implemented to couple models, such as SWAT-N, LandscapeDNDC-CMF, APSIM,
74 SWAT-DayCent, and CNMM-DNDC (e.g., Pohlert *et al.*, 2007; Haas *et al.*, 2012; Holzworth *et al.*, 2014; Wu *et al.*, 2016;
75 Zhang *et al.*, 2016; Zhang *et al.*, 2018b). The models derived from SWAT were all based on semi-distributed hydrological
76 models using hydrologic response units and did not perform better in estimating non-point source pollution (e.g., Pohlert *et*
77 *al.*, 2007; Bosch *et al.*, 2011 ;Wu *et al.*, 2016). A coupler was used to couple two models for LandscapeDNDC-CMF, which
78 realized the simulation of horizontal movement of water and nutrients (e.g., Haas *et al.*, 2012; Klatt *et al.*, 2017; Schroeck *et*
79 *al.*, 2019). Compared with other models, the Catchment Nutrient Management Model - DeNitrification-DeComposition
80 (CNMM-DNDC), which was established by incorporating the core biogeochemical processes of DNDC into the
81 hydrological framework of the CNMM, was validated at a catchment with complex landscapes in the subtropical region and
82 showed good performance for simultaneously simulating various variables, including ecosystem productivity, hydrological
83 nitrogen losses and nitrate discharge in streams, and emissions of gaseous carbon and nitrogenous gases (Zhang *et al.*,
84 2018b). Therefore, the CNMM-DNDC has the capacity to simulate the various variables closely related to both productivity
85 and environmental hazards.

86 However, as a process-oriented hydro-biogeochemical model designed to be applicable to different climate zones, soils,
87 land uses and field management practices, CNMM-DNDC testing is still lacking due to limited observations for model
88 validation. In this study, the model was applied to a catchment in a seasonally frozen region located on the eastern Tibetan
89 Plateau with the land use types of alpine wetlands, meadows and forests to test its ability to simulate hydro-biogeochemical
90 processes. However, scientific descriptions of soil thermal dynamics due to freeze-thaw cycles are still lacking for the
91 CNMM-DNDC. This gap may hinder model application in seasonally frozen regions, which account for 56% of the exposed
92 land surface of the Northern Hemisphere (Jiang *et al.*, 2020). In addition, the soil freeze-thaw cycles that occur in these mid-
93 high latitude regions exert important influences on soil thermal dynamics, as well as on related hydrological processes, thus
94 increasing the availability of substrates and stimulating the processes of CH₄ and N₂O production and emissions in soils (e.g.,
95 Song *et al.*, 2019). Therefore, we hypothesize that adding the missing scientific processes of soil thermal dynamics into the
96 internal model program codes can improve the performance of the CNMM-DNDC in simulating the soil thermal dynamics,
97 hydrological processes and CH₄ and N₂O fluxes in seasonally frozen regions. Filling this gap is especially necessary to
98 broaden model applicability.

99 To test the above hypothesis, the catchment simulation in the Rierlangshan was conducted using a unique experimental
100 dataset, which was obtained by Zhang *et al.* (2018a, 2019) and Yao *et al.* (2019) for the catchment that involved three typical
101 alpine ecosystems, wetlands, meadows and forests, on the eastern Tibetan Plateau. The aims of this study were to (i) attempt
102 to address the gap in the CNMM-DNDC by improving the scientific processes of soil thermal dynamics for seasonally
103 frozen regions and (ii) compare the performances of the original and modified models in simulating the soil profile
104 temperature, topsoil moisture and CH₄ and N₂O fluxes in three typical alpine ecosystems in the Rierlangshan catchment with
105 field observations. Therefore, the validated model with modifications provides a mechanism for not only interpreting
106 observations but also predicting the CH₄ and N₂O fluxes in alpine ecosystems.

107 **2 Materials and methods**

108 **2.1 Model description**

109 **2.1.1 Overview of the CNMM-DNDC model**

110 The CNMM-DNDC is a process-oriented model developed for simulating hydro-biogeochemical interactions at the
111 catchment or site scale, and this model is designed following the basic theories of physics, chemistry, and biogeochemistry
112 and has the capacity to simulate the complex transport and transformation of water, nitrogen and carbon in terrestrial
113 ecosystems under both aerobic and anaerobic conditions. The model can be applied to simultaneously quantify ecosystem
114 productivity, net emissions of nitrogen and carbon gases and hydrological nitrogen losses through soil leaching and
115 discharge in streams from an entire catchment or individual landscape unit (Zhang *et al.*, 2018b). The model was established
116 to address the bottleneck issue associated with most biogeochemical models, i.e., the inability to simulate the lateral flows of
117 water and nutrients, by incorporating the core biogeochemical processes of DNDC (including the processes of
118 decomposition, nitrification, denitrification and fermentation) into the hydrological framework of the CNMM, which is fully
119 distributed. For the new generation of biogeochemical models, the microbial ecology was integrated into the biogeochemical
120 models, which represents direct microbial control over decomposition, such as MOMOS (Pansu *et al.*, 2010; Treseder *et al.*,
121 2011; Todd-Brown *et al.*, 2012; Pansu *et al.*, 2014). The biogeochemical processes simulated by the DNDC were generally
122 based on first-order kinetics for decomposition and Michaelis-Menten kinetics of two substrates for nitrification and
123 denitrification, which only the parameterized growth and death of nitrifiers and denitrifiers were considered (Li, 2000).
124 However, due to the global application and validation of DNDC (e.g., Chen *et al.*, 2008; Giltrap *et al.*, 2010; Cui *et al.*, 2014,
125 Zhang *et al.*, 2015), the biogeochemical processes of DNDC were selected in the CNMM-DNDC despite some deficiencies
126 in simulating microbial biomass.

127 The simulated soil depth (including bedrock) is user-defined. The temporal and spatial resolutions are also user-
128 defined according to the driving data of climate (generally in 3 hours) and digital elevation model (DEM). The soil moisture
129 was calculated based on the mass balance of precipitation, irrigation, evapotranspiration, vertical flow, lateral flow and water

130 from a rising water table. The total water that can be infiltrated during each time step was determined by a defined maximum
131 infiltration rate. Darcy's law was applied for predicting the vertical water flow in the soil profile. A cell-by-cell approach
132 using a kinematic approximation was applied to route the saturated overland and subsurface flow based on DEM. The stream
133 flow was estimated using a cascade of linear channel reservoirs (Wigmosta *et al.*, 1994). For plant growth, gross primary
134 production was simulated using Farquhar *et al.* (1980) for C₃ and Collatz *et al.* (1992) for C₄, with annual primary
135 productivity calculated as the residue of gross primary production and autotrophic respiration. The processes related to the
136 production of N₂O include nitrification and denitrification, which occur simultaneously at aerobic and anaerobic microsites,
137 respectively. The concept of an "anaerobic balloon" was adopted to determine the microsites and allocate substrates for
138 nitrification and denitrification. The sizes of the aerobic (nitrification) and anaerobic (denitrification) microsites were
139 determined by the soil redox potential (Eh) using the Nernst equation (Li, 2007). The "hole in the pipe" concept was applied
140 to calculate N₂O production during nitrification, which is influenced by the soil moisture, temperature and pH (Li, 2016).
141 The production of N₂O during denitrification was predicted with Michaelis-Menten kinetics and Pirt functions following the
142 reaction chain of denitrification. The predicted CH₄ flux was influenced by CH₄ production, oxidation and transportation
143 derived from the module of fermentation in the DNDC (Li, 2007). Methane production and oxidation occurred
144 simultaneously and were determined by the sizes of the aerobic (production) and anaerobic (oxidation) microsites, which
145 were defined by an Eh calculator in terms of an "anaerobic balloon" ("CH₄ balloon") (Li, 2007). The predicted CH₄
146 production was calculated from the carbon substrates resulting from decomposed soil organic carbon (SOC) and plant root
147 biomass with the effects of soil temperature (Li, 2000, 2016). For more details, please see Li. (2000, 2007) and Zhang *et al.*
148 (2018b).

149 **2.1.2 Modifications of the CNMM-DNDC model**

150 In the CNMM-DNDC, the soil temperature was predicted by solving the one-dimensional heat conduction equation
151 with the implicit method of Crank-Nicholson. However, despite the simple parameterization used for the calculation of soil
152 heat capacity and thermal conductivity, the variations of soil temperature induced by the freeze-thaw cycles were also not
153 considered (Table S1 of the online supplementary materials), which inevitably hindered its application in seasonally frozen
154 regions. In this study, the CNMM-DNDC was modified by replacing the above soil thermal module by a physical based
155 module of Northern Ecosystem Soil Temperature (Zhang *et al.*, 2003; Deng *et al.*, 2014), which can explicitly describe the
156 energy exchange within the soil, the active layer dynamics and the soil thermal regime in the presence of freeze-thaw cycles.
157 These modifications are indispensable for accurately simulating freeze-thaw cycles in seasonally frozen regions, which are
158 crucial for characterizing the active layer and soil thermal dynamics, soil hydrology and nitrogen or carbon cycling in these
159 regions. Therefore, the CNMM-DNDC with and without the above modifications are hereafter referred to as the original and
160 modified model, respectively.

161 The modified thermal dynamics of the soil are calculated by the one-dimensional heat conduction equation (Eq. 1).
162 The equation is solved numerically by converting to an explicit form (Eqs. 2–4), which is more efficient for considering the

163 freeze-thaw cycles (Zhang *et al.*, 2003). In the above equations, C ($\text{J m}^{-3} \text{ }^\circ\text{C}^{-1}$), k ($\text{W m}^{-1} \text{ }^\circ\text{C}^{-1}$), T ($^\circ\text{C}$) and G (W m^{-2}) denote
164 the soil heat capacity, thermal conductivity, soil temperature and heat fluxes between layers, respectively. Both Z and D are
165 the thicknesses of the soil layer (m), Δt is the time step of the calculation, and l denotes the soil layer l . S is the internal heat
166 exchange due to freezing or thawing (W m^{-3}) when the soil temperature is around $0 \text{ }^\circ\text{C}$. The soil temperature changes
167 affected by freezing or thawing are determined on the basis of energy conservation, which indicate that the latent heat
168 released during freezing equalled the amount of heat required for the increased soil temperature and vice versa. The dynamic
169 soil heat capacity (C_l , $\text{J m}^{-3} \text{ }^\circ\text{C}^{-1}$) is the weighted average of the heat capacity for five constituents, including organic matter
170 ($C_{l, \text{OM}}$), minerals ($C_{l, \text{Min}}$), water ($C_{l, \text{Water}}$), ice ($C_{l, \text{Ice}}$) and air ($C_{l, \text{Air}}$) (Eq. 5). The values of heat capacity for organic matter,
171 minerals, water, ice and air were 2.5×10^6 , 2.0×10^6 , 4.2×10^6 , 2.1×10^6 and $1.2 \times 10^3 \text{ J m}^{-3} \text{ }^\circ\text{C}^{-1}$, respectively (Huang, 2000). The
172 weight is the relative volumetric fraction of each constituent ($\theta_{l, \text{OM}}$, $\theta_{l, \text{Min}}$, $\theta_{l, \text{Water}}$, $\theta_{l, \text{Ice}}$, $\theta_{l, \text{Air}}$) in the soil. The dynamic
173 thermal conductivity (k_l , $\text{W m}^{-1} \text{ }^\circ\text{C}^{-1}$) is calculated using the thermal conductivities of above five constituents (Eq. 6–13),
174 with values of 0.25 ($k_{l, \text{OM}}$), 2.9 ($k_{l, \text{Min}}$), 0.57 ($k_{l, \text{Water}}$), 2.2 ($k_{l, \text{Ice}}$) and 0.025 ($k_{l, \text{Air}}$) $\text{W m}^{-1} \text{ }^\circ\text{C}^{-1}$ for organic matter, minerals,
175 water, ice and air, respectively (Johansen, 1975). ST_l denotes the soil temperature of layer l ($^\circ\text{C}$). The upper and lower
176 boundary conditions of the thermal dynamics were determined by the surface energy balance and the defined geothermal
177 heat flux at a soil depth of 35 m.

$$C \frac{\partial T}{\partial t} = \frac{\partial}{\partial Z} \left(k \frac{\partial T}{\partial Z} \right) + S \quad (1)$$

$$C_l \frac{\Delta T_l}{\Delta t} = \frac{G_{l-1, l} - G_{l, l+1}}{D_l} + S_l \quad (2)$$

$$G_{l-1, l} = \frac{(0.5k_l + 0.5k_{l-1})(T_{l-1} - T_l)}{0.5D_{l-1} + 0.5D_l} \quad (3)$$

$$G_{l, l+1} = \frac{(0.5k_l + 0.5k_{l+1})(T_l - T_{l+1})}{0.5D_l + 0.5D_{l+1}} \quad (4)$$

$$C_l = C_{l, \text{OM}}\theta_{l, \text{OM}} + C_{l, \text{Min}}\theta_{l, \text{Min}} + C_{l, \text{Water}}\theta_{l, \text{Water}} + C_{l, \text{Ice}}\theta_{l, \text{Ice}} + C_{l, \text{Air}}\theta_{l, \text{Air}} \quad (5)$$

$$k_l = \frac{\theta_{l, \text{Water}}k_{l, \text{Water}} + F_{l, \text{Air}}\theta_{l, \text{Air}}k_{l, \text{Air_adj}} + F_{l, \text{OM+Min}}(\theta_{l, \text{OM}} + \theta_{l, \text{Min}})k_{l, \text{OM+Min}} + F_{l, \text{Ice}}\theta_{l, \text{Ice}}k_{l, \text{Ice}}}{\theta_{l, \text{Water}} + F_{l, \text{Air}}\theta_{l, \text{Air}} + F_{l, \text{OM+Min}}(\theta_{l, \text{OM}} + \theta_{l, \text{Min}}) + F_{l, \text{Ice}}\theta_{l, \text{Ice}}} \quad (6)$$

$$k_{l, \text{Air_adj}} = \begin{cases} k_{l, \text{Air}} + 0.0238e^{0.0536ST_l} & (\theta_{l, \text{Water}} > 0.09) \\ 0.418 \times (0.0615 + 1.96\theta_{l, \text{Water}}) & (\theta_{l, \text{Water}} \geq 0.09) \end{cases} \quad (7)$$

$$g_a = \begin{cases} 0.333 - \frac{0.298\theta_{l, \text{Air}}}{1 - \theta_{l, \text{OM}} - \theta_{l, \text{Min}}} & (\theta_{l, \text{Water}} > 0.09) \\ 0.013 + 0.944\theta_{l, \text{Water}} & (\theta_{l, \text{Water}} \geq 0.09) \end{cases} \quad (8)$$

$$g_c = 1.0 - 2.0g_a \quad (9)$$

$$k_{l, \text{OM+Min}} = k_{l, \text{OM}} \frac{\theta_{l, \text{OM}}}{\theta_{l, \text{OM}} + \theta_{l, \text{Min}}} + k_{l, \text{Min}} \frac{\theta_{l, \text{Min}}}{\theta_{l, \text{OM}} + \theta_{l, \text{Min}}} \quad (10)$$

$$F_{l, \text{Air}} = 0.333 \left(\frac{2.0}{1.0 + g_a \left(\frac{k_{l, \text{Air_adj}}}{k_{l, \text{Water}}} - 1.0 \right)} + \frac{1.0}{1.0 + g_c \left(\frac{k_{l, \text{Air_adj}}}{k_{l, \text{Water}}} - 1.0 \right)} \right) \quad (11)$$

$$F_{l, \text{OM+Min}} = 0.333 \left(\frac{2.0}{1.0 + 0.125 \left(\frac{k_{l, \text{OM+Min}}}{k_{l, \text{Water}}} - 1.0 \right)} + \frac{1.0}{1.0 + 0.75 \left(\frac{k_{l, \text{OM+Min}}}{k_{l, \text{Water}}} - 1.0 \right)} \right) \quad (12)$$

$$F_{l, \text{Ice}} = 0.333 \left(\frac{2.0}{1.0 + 0.125 \left(\frac{k_{l, \text{Ice}}}{k_{l, \text{Water}}} - 1.0 \right)} + \frac{1.0}{1.0 + 0.75 \left(\frac{k_{l, \text{Ice}}}{k_{l, \text{Water}}} - 1.0 \right)} \right) \quad (13)$$

178

179 Compared to the original thermal module, the internal heat exchange due to freezing or thawing (S) was included with
 180 improved algorithm for thermal conductivity (k). In addition, the one-dimensional heat conduction equation (Eq. 1) was
 181 solved by converting it to an explicit form in the modified model (Eqs. 2–4), while was solved with the implicit method in
 182 the original models (Table S1). The modified CNMM-DNDC was able to simulate the thermal dynamics in seasonally
 183 frozen regions as well as their impacts on biogeochemical processes, such as the emissions of nitrogen and carbon gases.

184 2.2 Catchment and field descriptions

185 The study area is the Rierlangshan catchment (34°02'N, 102°43'E) on the eastern Tibetan Plateau with an area of 189
 186 ha (Yao *et al.*, 2019). This catchment is located in the source region of the Pai-Lung River, which is a sub-branch of the
 187 upper Yangtze River (Zhang *et al.*, 2018a; 2019). This region is subject to a cold humid continental monsoon climate, and it
 188 had an annual mean air temperature of 1.6 ± 0.7 °C and average annual precipitation of 649 ± 94 mm in 1980–2012 as
 189 observed at the Zoige Meteorological Station (~80 km south of the catchment) (Ma *et al.*, 2018). The catchment consists of
 190 alpine wetlands, meadows and forests (Yao *et al.*, 2019). The alpine wetlands in the catchment are part of the Zoige wetland
 191 and are degraded due to anthropogenic drainage and climate warming (Dong *et al.*, 2010; Li *et al.*, 2014). Degraded alpine
 192 wetlands are commonly distributed throughout the Zoige wetland, and nearly 83% of the permanently inundated wetlands
 193 have been converted into “wet grassland” (Xiang *et al.*, 2009; Li *et al.*, 2014).

194 CH₄ and N₂O fluxes were manually measured once or twice per week using the gas chromatograph-based static opaque
 195 chamber method (Zhang *et al.*, 2018a) at three sites in alpine wetlands (34°02'6.53"N, 102°43'29.66"E, 3304 m a.s.l.),
 196 meadows (34°02'01"N, 102°43'28"E, 3326 m a.s.l.) and forests (34°01'47.13"N, 102°44'0.87"E, 3415 m a.s.l.) in the
 197 Rierlangshan catchment from 2013 to 2015 (Zhang *et al.*, 2018a; Yao *et al.*, 2019; Zhang *et al.*, 2019) (Fig. S1). Each
 198 chamber was wrapped with a layer of styrofoam and aluminium foil to mitigate temperature increases inside the enclosures
 199 due to the heating of solar radiation. The alpine wetland site is located at a slope base with a slope of 2°. The wetland has
 200 suffered from anthropogenic drainage and climate warming, and thus degraded to be seasonally inundated. The alpine
 201 meadow site neighbours the alpine wetland site, which is located on the north-facing slope with gradient of 11°. In addition,
 202 soil temperatures at different depths and topsoil moisture in the alpine wetlands, meadows and forests were observed daily

203 and twice per week, respectively. The details regarding the available field observations of the CH₄ and N₂O fluxes and the
204 relevant auxiliary variables are described in Table S2.

205 **2.3 Model simulation**

206 The modified CNMM-DNDC was applied in the Rierlangshan catchment with the three alpine ecosystems: wetlands,
207 meadows and forests. The dataset required for the catchment simulation included (1) a digital elevation model (DEM) with a
208 resolution of 30 × 30 m² from the geospatial data cloud (Fig. S1; <http://www.gscloud.cn/>); (2) a map of alpine ecosystems,
209 including wetlands, meadows and forests; (3) a climate dataset of 3-hour weather data (air temperature, precipitation, wind
210 speed, solar radiation, longwave radiation, and humidity), which were obtained from the meteorological station in the target
211 catchment for the years with field observations (2013.11–2015.10) and were adapted from the daily data at the Zoige
212 Meteorological Station (provided by the National Meteorological Information Center: <http://data.cma.cn/>; last access: 10th
213 June, 2020) for other years; (4) a soil properties dataset of the observed clay fraction, organic matter content, total nitrogen,
214 pH and bulk density of the three alpine ecosystems in 1 m soil profile (Ma *et al.*, 2018; Zhang *et al.*, 2018a; Yao *et al.*, 2019;
215 Zhang *et al.*, 2019; Table S3); and (5) a management practices dataset including grazing time and intensity for the alpine
216 wetlands and meadows (Table S3). In addition, other required soil inputs of field capacity, wilting point and saturated
217 hydrological conductivity were calculated by pedo-transfer functions (Li *et al.*, 2019; Table S4). The simulated soil depth
218 was defined as 35 m due to the lower boundary conditions of the thermal dynamics, which was set as the geothermal heat
219 flux at a soil depth of 35 m. The simulated soil profile (0–35 m depth) was divided into 23 layers, including the soil (0–1.5
220 m) and bedrock (1.5–35 m). The layer thicknesses of the soil (0–1.5 m) were 0.01, 0.05, 0.1 and 0.5 cm for the depth of 0–
221 0.1, 0.1–0.2, 0.2–1 and 1–1.5 m, respectively. The layer thicknesses of the bedrock (1.5–35 m) were 3.5 and 31m for the
222 depth of 1.5–4.0 and 4.0–35 m, respectively. The geothermal heat flux in the catchment was estimated at 0.053 W m⁻²
223 (Pollack and Chapman, 1977). For the target catchment, the soil water dynamics of the alpine ecosystems were determined
224 by the precipitation, evapotranspiration, infiltration, penetration and lateral flow. Using the database, a catchment simulation
225 of hydro-biogeochemical processes was performed with spatial and temporal resolutions of 30×30 m² and 3 hours,
226 respectively, by the modified CNMM-DNDC from 2012 to 2015, which could reflect the influences of hydrological
227 processes on soil water dynamics. Thus, the soil water dynamics of the seasonally inundated wetlands were determined by
228 the hydrological processes without any artificial disturbances in the catchment simulation.

229 **2.4 Statistics and analysis**

230 The statistical criteria applied for evaluating the model performance in this study included (i) the index of agreement
231 (IA), (ii) the Nash–Sutcliffe efficiency (NSE), and (iii) the determination coefficient (R^2) and slope of the zero-intercept
232 univariate linear regression (ZIR) of the observations against the simulations (e.g., Nash and Sutcliffe, 1970; Willmott and
233 Matsuura, 2005; Moriasi *et al.*, 2007; Congreves *et al.*, 2016; Jiang, 2010; Dubache *et al.*, 2019). A value of IA (0–1) closer
234 to 1 showed a better simulation. An NSE value (ranging from minus infinity to 1) closer to 1 was better. Better model

235 performance was indicated by a slope and an R^2 value that were both closer to 1 in a significant ZIR. The significance level
236 of the ZIR was indicated by the P value. For more details on these criteria, refer to the Eqs. S1–4 in Table S5. In addition,
237 the SPSS Statistics Client 19.0 (SPSS Inc., Chicago, USA) and Origin 8.0 (OriginLab, Northampton, MA, USA) software
238 packages were applied for the statistical analysis and graphical comparison.

239 **3 Results**

240 **3.1 Model validation**

241 **3.1.1 Soil temperature and moisture**

242 The profile soil temperatures were observed for alpine wetland and meadow, but only topsoil temperature was
243 observed for the alpine forest, which could be used for model validation. The simulated soil temperatures of the three typical
244 alpine ecosystems were significantly improved by including the scientific processes of soil thermal dynamics suitable for
245 seasonally frozen regions (Figs. 1 and S2). The simulated seasonal dynamics and magnitudes were consistent with those
246 from the field observations for various soil depths, with IA, NSE, and ZIR slopes and R^2 values of 0.91–1.00, 0.68–0.99,
247 0.83–1.09 and 0.73–1.00 for the three alpine ecosystems, respectively (Table 1). For the observed alpine wetlands and
248 meadows, the simulation showed that the freezing of soil started in early November and continued to the end of April in the
249 next year. The frozen depth reached a maximum in the middle of February. However, the simulated maximum frozen depths
250 for the observed alpine meadows (0.69–0.74 m) were approximately double those for the alpine wetlands (0.30–0.39 m) (Fig.
251 S3).

252 For the soil moisture, only topsoil moisture was observed in the three alpine ecosystems, which could be applied for
253 model validation. The simulated topsoil moisture dynamics were comparable to those from the field observations, with IA
254 and NSE values of 0.49–0.83 and -0.80–0.32 for the three alpine ecosystems, respectively (Fig. 2 and Table 1). In
255 comparison to the other alpine ecosystems, the alpine wetlands had higher soil moisture, which ranged from 0.41 to 0.98 and
256 from 0.38 to 0.93 for the observations and simulations in the water-filled pore space (WFPS), respectively. The soil moisture
257 values of the alpine meadows and forests were highly variable and depended on the variation trend in precipitation for both
258 observations and simulations. However, an underestimation of soil moisture in the winter period occurred for both alpine
259 meadows and forests due to a possible overestimation of evapotranspiration. The performances of the modified model in
260 simulating the soil profile temperature and topsoil moisture indicate that the modified CNMM-DNDC can generally predict
261 the soil thermal and topsoil moisture dynamics in the three alpine ecosystems, which is crucial for correctly simulating soil
262 hydrology, plant growth and biogeochemical processes.

263 3.1.2 Methane fluxes

264 The daily observed CH₄ emissions from the alpine wetlands were highly variable and showed a clear seasonal cycle,
265 with intensive CH₄ emissions from May to November and weak emissions in other periods (Fig. 3a). The observed alpine
266 meadows and forests functioned exclusively as sinks of atmospheric CH₄ with higher rates of uptake during the growing
267 season and lower uptake rates in the dormant season (Figs. 3b–c). The original model significantly overestimated CH₄
268 emissions from the alpine wetlands. The modified CNMM-DNDC accurately identified the functions of the sources or sinks
269 in the three alpine ecosystems and generally captured the magnitude and seasonal characteristics of the daily CH₄ fluxes,
270 with an IA of 0.57–0.88 for the three alpine ecosystems (Figs. 3a–c and Table 1). However, the CH₄ uptake rates during the
271 dormant season were obviously underestimated by the modified model at both sites, especially at the alpine forest site, which
272 was responsible for the underestimation of cumulative CH₄ uptake. The observed cumulative CH₄ emissions ranged from -
273 2.60 to 33.5 kg C ha⁻¹ yr⁻¹ and the modelled values ranged from -1.90 to 31.0 kg C ha⁻¹ yr⁻¹ (Fig. 4a). These results indicate
274 that the modified CNMM-DNDC well simulated the CH₄ fluxes of the three typical alpine ecosystems.

275 3.1.3 Nitrous oxide fluxes

276 The daily observed N₂O emissions from the alpine wetlands were higher than those from the alpine meadows but
277 lower than those from the alpine forests (Figs. 3d–f). Similar seasonal patterns of N₂O fluxes were observed for the three
278 alpine ecosystems with intensive emissions in the growing season. The N₂O emission peak during the dormant season was
279 observed in the alpine meadows, which was the major contributor to annual emissions. The modified CNMM-DNDC
280 generally captured the seasonal dynamics of daily N₂O fluxes with an IA of 0.26–0.47 for the three alpine ecosystems (Figs.
281 3d–f and Table 1), but the N₂O emissions from the alpine wetlands were significantly overestimated by the original model.
282 For the modified model, the simulated N₂O emissions from the alpine wetlands and forests showed obvious seasonal patterns
283 with higher emissions during the growing season, but no abrupt emission peak was captured at the end of the growing season
284 for the alpine wetlands. In addition, compared with the original model, the modified model captured the peak emissions that
285 occurred during the freeze-thaw period from the alpine meadows due to the death of microbes, but the dynamics of the peak
286 emissions were not well simulated. The observed cumulative N₂O emissions ranged from 0.14 to 0.58 kg N ha⁻¹ yr⁻¹ and the
287 modelled values ranged from 0.12 to 0.32 kg N ha⁻¹ yr⁻¹ (Fig. 4b). These results indicate that the modified CNMM-DNDC
288 has the potential to estimate N₂O emissions in seasonally frozen regions.

289 3.2 Annual aggregate emissions of CH₄ and N₂O

290 Annual aggregate emissions of CH₄ and N₂O in carbon dioxide (CO₂) equivalents were calculated for the three alpine
291 ecosystems from November 2013 to November 2014 for alpine wetlands and meadow and from April 2014 to April 2015 for
292 alpine forests, and the global warming potentials were 34 for CH₄ and 298 for N₂O on a 100-year time horizon (IPCC, 2013).
293 The simulated aggregate emissions by the modified model were 1.5, 0.015, and 0.061 Mg CO₂eq ha⁻¹ yr⁻¹ for the observed

294 alpine wetlands, meadows and forests, respectively, which were consistent with those from the field observations (1.6, 0.014,
295 and 0.15 Mg CO₂eq ha⁻¹ yr⁻¹ for the alpine wetlands, meadows and forests, respectively) (Fig. 4c). However, the original
296 model significantly overestimated the aggregate emissions due to the high predicted CH₄ and N₂O emissions. In comparison,
297 the observed seasonally inundated wetlands functioned as the sources of aggregate emissions of CH₄ and N₂O, but the
298 aggregate emissions from adjacent wet alpine meadows were much lower.

299 **4 Discussions**

300 **4.1 Model performance in simulating thermal dynamics**

301 The soil freeze-thaw cycles in seasonally frozen regions determine the soil profile temperature and hydrological
302 processes, which are key factors that regulate the cycling of nitrogen and carbon (e.g., Zhang *et al.*, 2015; Hugelius *et al.*,
303 2020). Therefore, improving the scientific processes of soil thermal dynamics in the presence of active layer dynamics is
304 essential for applying the CNMM-DNDC to simulate the biogeochemical processes in seasonally frozen regions, which are
305 sensitive and vulnerable to climate change and human activities (Hatano, 2019; Hugelius *et al.*, 2020; Jiang *et al.*, 2020). The
306 original model adopted a relatively simple module to calculate thermal transportation within the soil profile and did not
307 consider the effects of freeze-thaw cycles on soil temperature and moisture. The newly incorporated module was based on
308 explicit energy conservation and exchange in the soil profile and successfully captured the variations in soil temperature and
309 topsoil moisture for the three alpine ecosystems during the freeze-thaw period. The simulated lower soil frozen depth for the
310 observed alpine wetland was primarily attributed to the higher soil profile moisture level, as the thermal conductivity and
311 heat capacity for water-filled pores were higher than those for air-filled pores. In order to quantify the impacts of climate
312 change on the cycling of carbon and water on the regional and global scales, several large scale ecosystem models or
313 macroscale hydrological models, such as Terrestrial Ecosystem Model, Lund-Potsdam-Jena dynamic global vegetation
314 model and Variable Infiltration Capacity model, have been enhanced to simulate the soil thermal dynamics at northern high
315 latitude (e.g., Wania *et al.*, 2009; Zhuang *et al.*, 2001; Cuo *et al.*, 2015; Jiang *et al.*, 2020). In addition, the soil thermal
316 modules were also improved in some biogeochemical models, such as DNDC and Mobile-DNDC, to evaluate the influences
317 of climate warming on the biogeochemical processes in high latitude regions (e.g., Zhang *et al.*, 2003; de Bruijn *et al.*, 2009;
318 Wolf *et al.*, 2011; Zhang *et al.*, 2012; Deng *et al.*, 2014). Compared with the simulated soil profile temperatures by above
319 models at different scales, the simulations in this study by the modified CNMM-DNDC were equally well, especially for
320 deeper soil layers (e.g., Wania *et al.*, 2009). For the validated topsoil moisture in this study, the modified model generally
321 captured the variation trends, which were comparable with the performances of other models (e.g., de Bruijn *et al.*, 2009;
322 Wolf *et al.*, 2011; Cuo *et al.*, 2015). However, compared with the studies focused on simulating soil moisture (e.g., Ford *et al.*,
323 2014), further improvements are still required to improve the model performance in simulating the soil moisture. These
324 results indicate the efficiency of the incorporated module in simulating soil thermal and topsoil moisture dynamics in
325 seasonally frozen regions.

326 4.2 Model performance in simulating CH₄ fluxes

327 Compared with the annually inundated wetlands, the seasonally inundated wetlands had relatively low observed and
328 simulated CH₄ emissions due to the significant influences of the water table level on CH₄ emissions (e.g., Hatano, 2019;
329 Zhang *et al.*, 2019). The CH₄ emissions simulated by the CNMM-DNDC were determined by the processes of production,
330 oxidation and transpiration. The unsaturated soil with moisture levels ranging from 0.41 to 0.98 WFPS resulted in a small
331 CH₄ balloon and thus reduced CH₄ production. At the same time, relatively dry conditions caused the upper soil layer to act
332 as an efficient oxidative methanotrophic barrier for the diffusion of CH₄ from the subsoil and thus decreased CH₄ emissions
333 (Kandel *et al.*, 2018; Tan *et al.*, 2020). In addition, the highly fluctuating CH₄ emissions simulated by the modified model
334 were also attributed to the high dependency of CH₄ production on soil moisture, which controlled the size of the CH₄ balloon.
335 Theoretically, the CH₄ emissions simulated by the original model should not be higher than those simulated by the modified
336 model due to the lower predicted soil moisture level. The overestimated CH₄ emissions simulated by the original model were
337 mainly attributed to the overestimated soil temperature due to their influences on mineralized substrates for CH₄ production,
338 as well as the processes of CH₄ production. This result implies that global warming may trigger intensive CH₄ emissions
339 from degraded wetlands, which could partly serve as a trade-off for the decreased CH₄ emissions due to the lower water table
340 level in degraded wetlands (e.g., Gong *et al.*, 2020). For the studies focused on simulating CH₄ emissions from wetlands by
341 the large-scale ecosystem models, the model validation with field observation is difficult due to coarse spatial resolution (e.g.,
342 Zhuang *et al.*, 2004). For the biogeochemical model, such as DNDC, the dynamics of CH₄ emissions from wetland and
343 peatland in the northern permafrost regions were well simulated (Zhang *et al.*, 2012; Deng *et al.*, 2014), which showed
344 consistent seasonal variations and magnitudes as those in this study. Both observations and simulations showed that the CH₄
345 uptake in alpine forests was higher than that in alpine meadows, which was mainly attributed to the high SOC content of the
346 alpine forests in the simulation. Methane uptake by upland soils is a biological process governed by the availability of CH₄
347 and oxygen as well as the activity and quantity of methanotrophic bacteria in soils (e.g., Liu *et al.*, 2007; Zhang *et al.*, 2014).
348 In the model, the simulated CH₄ uptake was positively related to the SOC content, which is closely related to the population
349 size of methanotrophic bacteria. Thus, the SOC content primarily contributed to the differences in CH₄ uptake from alpine
350 meadows and forests, as the values for forests were more than twice of those for meadows (Table S3). As the simulated
351 dynamic characteristics of CH₄ uptake were primarily regulated by soil temperature and moisture, the inhibitory effects of
352 low soil temperature (< 0.0 °C) on CH₄ uptake rates resulted in obvious underestimations in the dormant season for both
353 alpine meadows and forests. Therefore, an improved parameterization for simulating CH₄ uptake under low soil temperatures
354 is required for the model to better capture the dynamics of CH₄ uptake in the dormant season.

355 4.3 Model performance in simulating N₂O fluxes

356 In comparison, the N₂O emissions from the alpine wetlands and forests were higher than those from the alpine
357 meadows for both the observations and simulations due to the high SOC content and nitrogen availability. Natural wetlands

358 are large carbon reserves and play a crucial role in mitigating global warming (e.g., Deng *et al.*, 2014; Kang *et al.*, 2020; Tan
359 *et al.*, 2020). The intentional drainage of annually inundated wetlands alters not only the water regime but also nutrient
360 availability (e.g., Hoffmann *et al.*, 2016). The simulated relatively low soil moisture for the alpine wetlands stimulated the
361 decomposition of SOC and nitrogen (or peat oxidation) under aerobic conditions, thus improving nitrogen mineralization for
362 nitrification and denitrification and enhancing N₂O emissions (e.g., Tan *et al.*, 2020; Zhang *et al.*, 2020). The intensive N₂O
363 emissions simulated by the original model resulted from the overestimated soil temperature for the alpine wetlands. Firstly,
364 as the presence of ice could impede the water movement, the water lateral flows were promoted by the original model due to
365 the neglecting of freeze-thaw cycles. These further resulted in the lower simulated soil moisture as compared with the
366 modified model (Fig. S4), which provided favorable oxygen conditions for N₂O production. Meanwhile, the simulated high
367 soil moisture by the modified model provided feasible anaerobic conditions for thoroughly denitrification. Secondly, higher
368 simulated soil temperature by the original model also facilitated the mineralization, which provided more available mineral
369 nitrogen. Field studies showed that high SOC concentrations could stimulate the processes of mineralization and nitrification
370 in the forests (e.g., Li *et al.*, 2005; Yao *et al.*, 2019). The model input of soil organic matter measured in the observed alpine
371 forests was more than twice that in the observed alpine meadows (Table S3). Thus, the high SOC content at the alpine forest
372 site provided more available nitrogen through mineralization and thus stimulated the nitrification processes in the simulation.
373 Furthermore, the seasonal grazing that occurred in the alpine meadows resulted in constant loss of available nitrogen and
374 thus hindered the N₂O emissions from the biological processes in the simulation. Field observations showed that the soil
375 freeze-thaw cycles occurred in seasonally frozen regions not only increased the availability of nitrogen and carbon substrates
376 by disrupting of soil aggregates but also affected the structure, population and activity of the microbes, and thus influencing
377 the emissions of N₂O (e.g., Song *et al.*, 2019). de Bruijn *et al.* (2009) have explored the combined mechanisms for
378 simulating freeze–thaw related N₂O emissions, which were the promoted anaerobiosis and denitrification due to reduced gas
379 diffusion derived from soil frost and snow cover, and the stimulated microbial growth due to easy decomposable organic
380 carbon and nitrogen derived from the dead microbes during freeze-thaw cycles. Wolf *et al.* (2011) introduced an impedance
381 factor to parameterize the reduced water flow between layers in the presence of ice, which could captured the freeze–thaw
382 related N₂O emissions for ungrazed steppe. In the CNMM-DNDC, threshold values of soil temperature were set to trigger
383 the death of microbes during the freezing period and stimulate the production of NO, N₂O and N₂ using substrates derived
384 from the dead microbes during the thawing period, which was similar to one of the mechanisms explored by de Bruijn *et al.*
385 (2009). However, compared with the simulated freeze–thaw related N₂O emissions by other studies, the simulated dynamics
386 of peak emissions due to freeze-thaw cycles in this study were inconsistent with those from the field observations. Thus,
387 improvements are required to incorporate some other effective mechanisms to better capture the dynamic characteristics. The
388 peak emissions during the freeze-thaw period were not captured by the original model due to the significantly overestimated
389 soil temperature. The low evaluation statistics for the daily fluxes, especially for the alpine forests, were also attributed to the
390 underestimation of background emissions, which resulted from both measurement errors due to low fluxes around detection
391 limits ($\pm 0.41 \text{ g N ha}^{-1} \text{ d}^{-1}$) and model deficiencies in the simulation of tight nitrogen cycling in natural ecosystems.

392 Compared with the empirical model, one key advantage of the process-oriented models is that the models are
393 independent of the local parameterization (Zhang *et al.*, 2015). In this study, default internal parameter combinations of
394 biogeochemical processes were used for the original and modified models, which have been applied in the catchment
395 simulation in the subtropical region (Zhang *et al.*, 2018b), due to the limited field observations (only one year) for both
396 calibration and validation. The biogeochemical processes were predicted by the first-order and Michaelis-Menten kinetics in
397 the CNMM-DNDC based on some defined parameters of flow fractionation. For instance, there are 17 parameters related
398 with N₂O emission in the module of denitrification (Table S6), which would inevitably increase the uncertainty of simulation.
399 Houska *et al.* (2017) found that hydro-biogeochemical models can be right for the wrong reasons, such as matching
400 greenhouse gas emissions while failing to simulate soil moisture, which emphasized the importance for simultaneous
401 validations of multi-variables. Thus, simultaneous validations of CH₄ and N₂O fluxes, as well as soil environment variables,
402 were necessary for comprehensive evaluation of the model performance. In addition, the microbial ecology was recently
403 recommended to be integrated into the biogeochemical model using a smaller number of well-defined kinetic parameters,
404 such as MOMOS (Pansu *et al.*, 2010; Treseder *et al.*, 2011). Therefore, direct control of microbial on biogeochemical
405 processes, such as the stoichiometry of decomposer, is required to be included in the CNMM-DNDC in near future. The
406 model performances of simulating various variables for three typical alpine ecosystems in the Rierlangshan catchment imply
407 that the modified CNMM-DNDC can be applied to predict the thermal dynamics and fluxes of CH₄ and N₂O from alpine
408 ecosystems in seasonally frozen regions.

409 **5 Conclusions**

410 To apply the process-oriented hydro-biogeochemical model Catchment Nutrient Management Model - DeNitrification-
411 DeComposition (CNMM-DNDC) in seasonally frozen regions, an improved module of soil thermal dynamics for describing
412 the soil thermal regime in the presence of freeze-thaw cycles was incorporated in this study. Using the unique experimental
413 dataset obtained in the Rierlangshan catchment with the typical alpine wetland, meadow and forest ecosystems, the modified
414 model was evaluated for simulating soil thermal dynamics (soil profile temperature), topsoil moisture and fluxes of methane
415 (CH₄) and nitrous oxide (N₂O) in seasonally frozen regions of the Tibetan Plateau. The modified CNMM-DNDC could
416 generally capture the seasonal dynamics and magnitudes of profile soil temperature, topsoil moisture and fluxes of CH₄ and
417 N₂O in seasonally frozen regions. Both the observed and simulated CH₄ and N₂O fluxes from three alpine ecosystems
418 indicate that the aggregate emissions of CH₄ and N₂O were highest for the wetland among three alpine ecosystems. The
419 intensive aggregate emissions of CH₄ and N₂O were regulated by the high soil moisture, which was primarily determined by
420 the CH₄ emissions. This study implies that a hydro-biogeochemical model, such as the modified CNMM-DNDC, are able to
421 predict soil thermal dynamics, topsoil moisture and fluxes of CH₄ and N₂O in seasonally frozen regions with an improved
422 physical-based soil thermal module.

423 **Data availability**

424 The model, input, output and code can be obtained from <http://doi.org/10.6084/m9.figshare.14685441>. All the observed data
425 sets used in this study can be available from the co-authors.

426 **Author contribution**

427 Zheng, X. and Zhang, W. contributed to developing the idea and enhancing the science of this study. Zhang, W. improved
428 the scientific processes of the model, implemented the model simulations and prepared the manuscript with contributions
429 from all co-authors. Li, S. improved the model structure for standard input. Yao, Z., Zhang, H., Ma, L., Wang, K., Wang, R.
430 and Liu, C. designed and carried out the field experiments. Han, S. collected and established the input database for modelling.
431 Deng, J and Li, Y contributed to the modification of the model and the improvement of the manuscript.

432 **Competing interests**

433 The authors declare that they have no conflict of interest.

434 **Acknowledgement**

435 This study was jointly supported by the National Key R&D Program of China (2016YFA0602303), the Chinese Academy of
436 Sciences (ZDBS-LY-DQC007), the National Key Scientific and Technological Infrastructure project “Earth System Science
437 Numerical Simulator Facility” (EarthLab), the National Natural Science Foundation of China (41603075) and

438 **References**

- 439 Bechmann, M., 2014. Long-term monitoring of nitrogen in surface and subsurface runoff from small agricultural dominated
440 catchments in Norway. *Agric. Ecosyst. Environ.* 198, 13–24.
- 441 Bosch, N., Allan, J., Dolan, D., Han, H., Richards, R., 2011. Application of the Soil and Water Assessment Tool for six
442 watersheds of Lake Erie: Model parameterization and calibration. *J. Great Lakes Res.* 37, 263–271.
- 443 Breuer, L., VachÉ, K., Julich, S., Frede, H., 2010. Current concepts in nitrogen dynamics for mesoscale catchments. *Hydrol.*
444 *Sci. J.-J. Sci. Hydrol.* 53, 1059–1074.
- 445 Canfield, D., Glazer, A., Falkowski, P., 2010. The evolution and future of Earth's nitrogen cycle. *Science* 330, 192–196.
- 446 Castellano, M., Lewis, D., Kaye, J., 2013. Response of soil nitrogen retention to the interactive effects of soil texture,
447 hydrology, and organic matter. *J. Geophys. Res.-Biogeosci.* 118, 280–290.
- 448 Chen, D., Li, Y., Grace, P., Mosier, A., 2008. N₂O emissions from agricultural lands: a synthesis of simulation approaches.
449 *Plant Soil* 309, 169–189.
- 450 Cheng, K., Ogle, S., Parton, W., Pan, G., 2014. Simulating greenhouse gas mitigation potentials for Chinese Croplands using
451 the DAYCENT ecosystem model. *Glob. Change Biol.* 20, 948–962.
- 452 Collatz, G., Ribas-Carbo, M., Berry, J., 1992. Coupled photosynthesis-stomatal conductance model for leaves of C₄ plants,
453 *Aust. J. Plant Physiol.*, 19, 519–538.

454 Collins, A., Zhang, Y., Winter, M., Inman, A., Jones, J., Johnes, P., Cleasby, W., Vrain, E., Lovett, A., Noble, L., 2016.
455 Tackling agricultural diffuse pollution: What might uptake of farmer-preferred measures deliver for emissions to water
456 and air? *Sci. Total Environ.* 547, 269–281.

457 Congreves, K., Grant, B., Dutta, B., Smith, W., Chantigny, M., Rochette, Desjardins, R., 2016. Prediction ammonia
458 volatilization after field application of swine slurry: DNDC model development, *Agric. Ecosyst. Environ.* 219, 179–189.

459 Cui, Z., Zhang, H., Chen, X., Zhang, C., Ma, W., Huang, C., Zhang, W., Mi, G., Miao, Y., Li, X., Gao, Q., Yang, J., Wang,
460 Z., Ye, Y., Guo, S., Lu, J., Huang, J., Lv, S., Sun, Y., Liu, Y., Peng, X., Ren, J., Li, S., Deng, X., Shi, X., Zhang, Q.,
461 Yang, Z., Tang, L., Wei, C., Jia, L., Zhang, J., He, M., Tong, Y., Tang, Q., Zhong, X., Liu, Z., Cao, N., Kou, C., Ying,
462 H., Yin, Y., Jiao, X., Zhang, Q., Fan, M., Jiang, R., Zhang, F., Dou, Z., 2018. Pursuing sustainable productivity with
463 millions of smallholder farmers. *Nature* 555, 363–366.

464 Cui, F., Zheng, X., Liu, C., Wang, K., Zhou, Z., Deng, J., 2014. Assessing biogeochemical effects and best management
465 practice for a wheat-maize cropping system using the DNDC model. *Biogeosciences* 11, 91–107.

466 Cuo, L., Zhang, Y., Bohn, T., Zhao, L., Li, J., Liu, Q., Zhou, B., 2015. Frozen soil degradation and its effects on surface
467 hydrology in the northern Tibetan Plateau. *J. Geophys. Res. Atmos.* 120, 8276–8298.

468 de Bruijn, A.M.G., Butterbach-Bahl, K., Blagodatsky, S., Grote, R., 2009. Model evaluation of different mechanisms driving
469 freeze–thaw N₂O emissions. *Agric. Ecosyst. Environ.* 133, 196–207.

470 Deng, J., Li, C., Frolking, S., Zhang, Y., Bäckstrand, K., Crill, P., 2014. Assessing effects of permafrost thaw on C fluxes
471 based on multiyear modeling across a permafrost thaw gradient at Stordalen, Sweden. *Biogeosciences* 11, 4753–4770.

472 Dong, Z., Hu, G., Yan, C., Wang, W., Lu, J., 2010. Aeolian desertification and its causes in the Zoige Plateau of China’s
473 Qinghai–Tibetan Plateau. *Environ. Earth Sci.* 59, 1731–1740.

474 Dubache, G., Li, S., Zheng, X., Zhang, W., Deng, J., 2019. Modeling ammonia volatilization following urea application to
475 winter cereal fields in the United Kingdom by improving a biogeochemical model, *Sci. Total Environ.* 660, 1403–1418.

476 Farquhar, G., Caemmerer, S., Berry, J., 1980. A biochemical model of photosynthetic CO₂ assimilation in leaves of C₃
477 species. *Planta*, 149, 78–90.

478 Fenner, N., Freeman, C., 2011. Drought-induced carbon loss in peatlands. *Nat. Geosci.* 4, 895–900.

479 Foereid, B., Barthram, G., Marriott, C., 2007. The CENTURY model failed to simulate soil organic matter development in
480 an acidic grassland. *Nutr. Cycl. Agroecosyst.* 78, 143–153.

481 Ford, T., Harris, E., Quiring, S., 2014. Estimating root zone soil moisture using near-surface observations from SMOS.
482 *Hydrol. Earth Syst. Sci.* 18, 139–154.

483 Galloway, J., Dentener, F., Capone, D., Boyer, E., Howarth, R., Seitzinger, S., Asner, G., Cleveland, C., Green, P., Holland,
484 E., Karl, D., Michaels, A., Porter, J., Townsend, A., Vorosmarty, C., 2004. Nitrogen Cycles: past, present, and future.
485 *Biogeochemistry* 70, 153–226.

486 Galloway, J., Townsend, A., Erisman, J., Bekunda, M., Cai, Z., Freney, J., Martinelli, L., Seitzinger, S., Sutton, M., 2008.
487 Transformation of the nitrogen cycle: recent trends, questions, and potential solutions. *Science* 320, 889–892.

488 Giltrap, D.L., Li, C., Saggar, S., 2010. DNDC: A process-based model of greenhouse gas fluxes from agricultural soils.
489 *Agric. Ecosyst. Environ.* 136, 292–300.

490 Gong, Y., Wu, J., Vogt, J., Ma, W., 2020. Greenhouse gas emissions from peatlands under manipulated warming, nitrogen
491 addition, and vegetation composition change: a review and data synthesis. *Environ. Rev.* 28, 428–437.

492 Haas, E., Klatt, S., Fröhlich, A., Kraft, P., Werner, C., Kiese, R., Grote, R., Breuer, L., Butterbach-Bahl, K., 2012.
493 LandscapeDNDC: a process model for simulation of biosphere–atmosphere–hydrosphere exchange processes at site and
494 regional scale. *Landsc. Ecol.* 28, 615–636.

495 Hatano, R., 2019. Impact of land use change on greenhouse gases emissions in peatland: a review. *Int. Agrophys.* 33, 167–
496 173.

497 Holzworth, D., Huth, N., deVoil, P., Zurcher, E., Herrmann, N., McLean, G., Chenu, K., van Oosterom, E., Snow, V.,
498 Murphy, C., Moore, A., Brown, H., Whish, J., Verrall, S., Fainges, J., Bell, L., Peake, A., Poulton, P., Hochman, Z.,
499 Thorburn, P., Gaydon, D., Dalgliesh, N., Rodriguez, D., Cox, H., Chapman, S., Doherty, A., Teixeira, E., Sharp, J.,
500 Cichota, R., Vogeler, I., Li, F., Wang, E., Hammer, G., Robertson, M., Dimes, J., Whitbread, A., Hunt, J., van Rees, H.,
501 McClelland, T., Carberry, P., Hargreaves, J., MacLeod, N., McDonald, C., Harsdorf, J., Wedgwood, S., Keating, B.,
502 2014. APSIM – Evolution towards a new generation of agricultural systems simulation. *Environ. Modell. Softw.* 62,
503 327–350.

504 Houska, T., Kraus, D., Kiese, R., Breuer, L., 2017. Constraining a complex biogeochemical model for CO₂ and N₂O
505 emission simulations from various land uses by model–data fusion. *Biogeosciences* 14, 3487–3508.

506 Huang, C., 2000. *Soil Science*. China Agriculture Press, Beijing. Pp. 125. (In Chinese)

507 Hugelius, G., Loisel, J., Chadburn, S., Jackson, R., Jones, M., MacDonald, G., Marushchak, M., Olefeldt, D., Maara, P.,
508 Siewert, M., Treat, C., Turetsky, M., Voigt, C., Yu, Z., 2020. Large stocks of peatland carbon and nitrogen are
509 vulnerable to permafrost thaw. *Proc. Natl. Acad. Sci. U. S. A.* doi: 10.1073/pnas.1916387117

510 Intergovernmental Panel on Climate Change (IPCC): *Climate Change 2013: The Physical Science Basis, Contribution of*
511 *Working Group I to the Fifth Assessment Report of the Intergovernmental Panel on Climate Change* (eds. Stocker TF,
512 Qin D, Plattner G-K, et al.), Cambridge University Press, Cambridge, United Kingdom and New York, NY, USA, 2013.

513 Jiang, H., Yi, Y., Zhang, W., Yang, K., Chen, D., 2020. Sensitivity of soil freeze/thaw dynamics to environmental conditions
514 at different spatial scales in the central Tibetan Plateau. *Sci. Total Environ.* 734, 139261. doi:
515 org/10.1016/j.scitotenv.2020.139261

516 Jiang, Z., 2010. Analysis on the establishment conditions of the square sum decomposition formular of regression model, *J.*
517 *Industr. Techn. Econ.* 29(4), 116–119 (in Chinese).

518 Johansen, O., 1975. *Thermal conductivity of soils*. Ph.D. thesis, Univ. of Trondheim, Trondheim, Norway.

519 Ju, X., Xing, G., Chen, X., Zhang, S., Zhang, L., Liu, X., Cui, Z., Yin, B., Christie, P., Zhu, Z., Zhang, F., 2009. Reducing
520 environmental risk by improving N management in intensive Chinese agricultural systems. *Proc. Natl. Acad. Sci. U.*
521 *S. A.* 106, 3041–3046.

522 Kandel, T., Lærke, P., Elsgaard, L., 2018. Annual emissions of CO₂, CH₄ and N₂O from a temperate peat bog: comparison of
523 an undrained and four drained sites under permanent grass and arable crop rotations with cereals and potato. *Agric. For.*
524 *Meteorol.* 256–257, 470–481.

525 Kang, X., Li, Y., Wang, J., Yan, L., Zhang, X., Wu, H., Yan, Z., Zhang, K., Hao, Y., 2020. Precipitation and temperature
526 regulate the carbon allocation process in alpine wetlands: quantitative simulation. *J. Soils Sediments* 20, 3300–3315.

527 Keiluweit, M., Wanzek, T., Kleber, M., Nico, P., Fendorf, S., 2017. Anaerobic microsites have an unaccounted role in soil
528 carbon stabilization. *Nat. Commun.* 8. doi: 10.1038/s41467-017-01406-6

529 Klatt, S., Kraus, D., Kraft, P., Breuer, L., Wlotzka, M., Heuveline, V., Haas, E., Kiese, R., Butterbach-Bahl, K., 2017.
530 Exploring impacts of vegetated buffer strips on nitrogen cycling using a spatially explicit hydro-biogeochemical
531 modeling approach. *Environ. Modell. Softw.* 90, 55–67.

532 Li, B., Yu, Z., Llang, Z., Song, K., Li, H., Wang, Y., Zhang, W., Acharya, K., 2014. Effects of climate variations and human
533 activities on runoff in the Zoige alpine wetland in the eastern edge of the Tibetan Plateau. *J. Hydrol. Eng.* 19, 1026–
534 1035.

535 Li, C., 2000. Modeling trace gas emissions from agricultural ecosystems. *Nutr. Cycl. Agroecosyst.* 58, 259–276.

536 Li, C., 2007. Quantifying greenhouse gas emissions from soils: scientific basis and modeling approach. *Soil Sci. Plant Nutr.*
537 53, 344–352.

538 Li, C., 2016. *Biogeochemistry: Scientific Fundamentals and Modelling Approach*. Tsinghua University Press, Beijing. Pp.
539 530. (In Chinese)

540 Li, C., Frolking, S., Butterbach-Bahl, K., 2005. Carbon sequestration in arable soils is likely to increase nitrous oxide
541 emissions, offsetting reductions in climate radiative forcing. *Clim. Change* 72, 321–338.

542 Li, S., Zheng, X., Zhang, W., Han, S., Deng, J., Wang, K., Wang, R., Yao, Z., Liu, C., 2019. Modeling ammonia
543 volatilization following the application of synthetic fertilizers to cultivated uplands with calcareous soils using an
544 improved DNDC biogeochemistry model. *Sci. Total Environ.* 660, 931–946.

545 Li, Y., White, R., Chen, D., Zhang, J., Li, B., Zhang, Y., Huang, Y., Edis, R., 2007. A spatially referenced water and
546 nitrogen management model (WNMM) for (irrigated) intensive cropping systems in the North China Plain. *Ecol. Model.*
547 203, 395–423.

548 Liu, C., Holst, J., Brüggemann, N., Butterbach-Bahl, K., Yao, Z., Yue, J., Han, S., Han, X., Krümmelbein, J., Horn, R.,
549 Zheng, X., 2007. Winter-grazing reduces methane uptake by soils of a typical semi-arid steppe in Inner Mongolia,
550 China. *Atmos. Environ.* 41, 5948–5958.

551 Liu, S., Xie, Z., Zeng, Y., Liu, B., Li, R., Wang, Y., Wang, L., Qin, P., Jia, B., Xie, J., 2019. Effects of anthropogenic
552 nitrogen discharge on dissolved inorganic nitrogen transport in global rivers. *Glob. Change Biol.* 25, 1493–1513.

553 Ma, L., Yao, Z., Zheng, X., Zhang, H., Wang, K., Zhu, B., Wang, R., Zhang, W., Liu, C., 2018. Increasing grassland
554 degradation stimulates the non-growing season CO₂ emissions from an alpine meadow on the Qinghai-Tibetan Plateau.
555 *Environ. Sci. Pollut. Res.* 25, 26576–26591.

556 McClain, M., Boyer, E., Dent, C., Gergel, S., Grimm, N., Groffman, P., Hart, S., Harvey, J., Johnston, C., Mayorga, E., 2003.
557 Biogeochemical hot spots and hot moments at the interface of terrestrial and aquatic ecosystems. *Ecosystems* 6, 301–
558 312.

559 Moriasi, D., Arnold, J., Van Liew, M., Bingner, R., Harmel, R., Veith, T., 2007. Model evaluation guidelines for systematic
560 quantification of accuracy in watershed simulation, *T. Am. Soc. Agr. Biol. Eng.* 50, 885–900.

561 Nash, J., Sutcliffe, J., 1970. River flow forecasting through conceptual models: part I- a discussion of principles, *J. Hydrol.*
562 10, 282–290.

563 Pansu, M., Sarmiento, L., Rujano, M., Ablan, M., Acevedo, D., Bottner, P., 2010. Modelling Organic transformations by
564 Micro-Organisms of Soils in six contrasting ecosystems: validation of the MOMOS model. *Glob. Biogeochem. Cycl.* 24,
565 GB1008. doi: org/10.1029/2009GB003527

566 Pansu, M., Machado, D., Bottner, P., Sarmiento, L., 2014. Modelling microbial exchanges between forms of soil nitrogen in
567 contrasting ecosystems. *Biogeosciences* 11, 915–927.

568 Piao, S., Fang, J., Ciais, P., Peylin, P., Huang, Y., Sitch, S., Wang, T., 2009. The carbon balance of terrestrial ecosystems in
569 China. *Nature* 458, 1009–1013.

570 Pohlert, T., Huisman, J., Breuer, L., Frede, H., 2007. Integration of a detailed biogeochemical model into SWAT for
571 improved nitrogen predictions—Model development, sensitivity, and GLUE analysis. *Ecol. Model.* 203, 215–228.

572 Pollack, H., Chapman, D., 1977. On the regional variation of heat flow, geotherms, and lithospheric thickness.
573 *Tectonophysics* 38, 279–296.

574 Schroeck, A., Gaube, V., Haas, E., Winiwarter, W., 2019. Estimating nitrogen flows of agricultural soils at a landscape level
575 - A modelling study of the Upper Enns Valley, a long-term socio-ecological research region in Austria. *Sci. Total*
576 *Environ.* 665, 275–289.

577 Schuur, E., McGuire, A., Schadel, C., Grosse, G., Harden, J., Hayes, D., Hugelius, G., Koven, C., Kuhry, P., Lawrence, D.,
578 Natali, S., Olefeldt, D., Romanovsky, V., Schaefer, K., Turetsky, M., Treat, C., Vonk, J., 2015. Climate change and the
579 permafrost carbon feedback. *Nature* 520, 171–179.

580 Seitzinger, S., 2008. Nitrogen cycle - Out of reach. *Nature* 452, 162–163.

581 Song, L., Yao, Y., Lin, L., Gao, W., Cai, T., Liang, H., Gao, D., 2019. The potential source of nitrous oxide in the pristine
582 riparian marsh during freeze-thaw cycles, case study in Northeast China. *Ecol. Eng.* 134, 18–25.

583 Tan, L., Ge, Z., Zhou, X., Li, S., Li, X., Tang, J., 2020. Conversion of coastal wetlands, riparian wetlands, and peatlands
584 increases greenhouse gas emissions: a global meta-analysis. *Glob. Change Biol.* 26, 1638–1653.

585 Todd-Brown, K., Hopkins, F., Kivlin, S., Jennifer, M., Talbot, J., Allison, S., 2012. A framework for representing microbial
586 decomposition in coupled climate models. *Biogeochemistry* 109, 19–33.

587 Treseder, K., Balsler, T., Bradford, M., Brodie, E., Dubinsky, E., Eviner, V., Hofmockel, K., Lennon, J., Levine, U.,
588 MacGregor, B., Pett-Ridge, J., Waldrop, M., 2011. Integrating microbial ecology into ecosystem models: challenges
589 and priorities. *Biogeochemistry* 109, 7–18.

590 Vereecken, H., Schnepf, A., Hopmans, J., Javaux, M., Or, D., Roose, T., Vanderborght, J., Young, M., Amelung, W.,
591 Aitkenhead, M., Allison, S., Assouline, S., Baveye, P., Berli, M., Brüggemann, N., Finke, P., Flury, M., Gaiser, T.,
592 Govers, G., Ghezzehei, T., Hallett, P., Hendricks Franssen, H., Heppell, J., Horn, R., Huisman, J., Jacques, D., Jonard,
593 F., Kollet, S., Lafolie, F., Lamorski, K., Leitner, D., McBratney, A., Minasny, B., Montzka, C., Nowak, W., Pachepsky,
594 Y., Padarian, J., Romano, N., Roth, K., Rothfuss, Y., Rowe, E., Schwen, A., Šimůnek, J., Tiktak, A., Van Dam, J., van
595 der Zee, S., Vogel, H., Vrugt, J., Wöhling, T., Young, I., 2016. Modeling Soil Processes: Review, Key Challenges, and
596 New Perspectives. *Vadose Zone J.* 15, doi:10.2136/vzj2015.2009.0131.

597 Wania, R., Ross, I., Prentice, I., 2009. Integrating peatlands and permafrost into a dynamic global vegetation model: 1.
598 Evaluation and sensitivity of physical land surface processes. *Glob. Biogeochem. Cycl.* 23, GB3014,
599 doi:10.1029/2008GB003412.

600 Wigmosta, M., Vail, L., Lettenmaier, D., 1994. A distributed hydrology-vegetation model for complex terrain. *Water Resour.*
601 *Res.*, 30, 1665–1679.

602 Willmott, C., Matsuura, K., 2005. Advantages of the mean absolute error (MAE) over the root mean square error (RMSE)
603 in assessing average model performance, *Clim. Res.*, 30, 79–82.

604 Wolf, B., Kiese, R., Chen, W., Grote, R., Zheng, X., Butterbach-Bahl, K., 2011. Modelling N₂O emissions from steppe in
605 Inner Mongolia, China, with consideration of spring thaw and grazing intensity. *Plant Soil* 350, 297–310.

606 Wu, Y., Liu, S., Qiu, L., Sun, Y., 2016. SWAT-DayCent coupler: An integration tool for simultaneous hydro-
607 biogeochemical modeling using SWAT and DayCent. *Environ. Modell. Softw.* 86, 81–90.

608 Xiang, S., Guo, R., Wu, N., Sun, S., 2009. Current status and future prospects of Zoige Marsh in Eastern Qinghai-Tibet
609 Plateau. *Ecol. Eng.* 35, 553–562.

610 Yao, Z., Ma, L., Zhang, H., Zheng, X., Wang, K., Zhu, B., Wang, R., Wang, Y., Zhang, W., Liu, C., Butterbach-Bahl, K.,
611 2019. Characteristics of annual greenhouse gas flux and NO release from alpine meadow and forest on the eastern
612 Tibetan Plateau. *Agric. For. Meteorol.* 272–273, 166–175.

613 Zhang, H., Yao, Z., Ma, L., Zheng, X., Wang, R., Wang, K., Liu, C., Zhang, W., Zhu, B., Tang, X., Hu, Z., Han, S., 2019.
614 Annual methane emissions from degraded alpine wetlands in the eastern Tibetan Plateau. *Sci. Total Environ.* 657,
615 1323–1333.

616 Zhang, H., Yao, Z., Wang, K., Zheng, X., Ma, L., Wang, R., Liu, C., Zhang, W., Zhu, B., Tang, X., Hu, Z., Han, S., 2018a.
617 Annual N₂O emissions from conventionally grazed typically alpine grass meadows in the eastern Qinghai-Tibetan
618 Plateau. *Sci. Total Environ.* 625, 885–899.

619 Zhang, W., Li, Y., Zhu, B., Zheng, X., Liu, C., Tang, J., Su, F., Zhang, C., Ju, X., Deng, J., 2018b. A process-oriented hydro-
620 biogeochemical model enabling simulation of gaseous carbon and nitrogen emissions and hydrologic nitrogen losses
621 from a subtropical catchment. *Sci. Total Environ.* 616–617, 305–317.

622 Zhang, W., Liu, C., Zheng, X., Fu, Y., Hu, X., Cao, G., Butterbach-Bahl, K., 2014. The increasing distribution area of zokor
623 mounds weaken greenhouse gas uptakes by alpine meadows in the Qinghai–Tibetan Plateau. *Soil Biol. Biochem.* 71,
624 105–112.

625 Zhang, W., Liu, C., Zheng, X., Wang, K., Cui, F., Wang, R., Li, S., Yao, Z., Zhu, J., 2019. Using a modified DNDC
626 biogeochemical model to optimize field management of a multi-crop (cotton, wheat, and maize) system: a site-scale
627 case study in northern China. *Biogeosciences* 16, 2905–2922.

628 Zhang, W., Liu, C., Zheng, X., Zhou, Z., Cui, F., Zhu, B., Haas, E., Klatt, S., Butterbach-Bahl, K., Kiese, R., 2015.
629 Comparison of the DNDC, LandscapeDNDC and IAP-N-GAS models for simulating nitrous oxide and nitric oxide
630 emissions from the winter wheat-summer maize rotation system. *Agric. Syst.* 140, 1–10.

631 Zhang, W., Wang, J., Hu, Z., Li, Y., Yan, Z., Zhang, X., Wu, G., Yan, L., Zhang, K., Kang, X., 2020. The primary drivers of
632 greenhouse gas emissions along the water table gradient in the Zoige alpine peatland. *Water Air Soil Pollut.* 231: 224.
633 doi: org/10.1007/s11270-020-04605-y

634 Zhang, Y., Chen, W., Cihlar, J., 2003. A process-based model for quantifying the impact of climate change on permafrost
635 thermal regimes. *J. Geophys. Res.-Atmos.* 108, 4695.

636 Zhang, Y., Sachs, T., Li, C., Boike, J., 2012. Upscaling methane fluxes from closed chambers to eddy covariance based on a
637 permafrost biogeochemistry integrated model. *Glob. Change Biol.* 18, 1428–1440.

638 Zhang, Y., Shao, Q., Ye, A., Xing, H., Xia, J., 2016. Integrated water system simulation by considering hydrological and
639 biogeochemical processes: model development, with parameter sensitivity and autocalibration. *Hydrol. Earth Syst. Sci.*
640 20, 529–553.

641 Zhu, Q., Castellano, M., Yang, G., 2018. Coupling soil water processes and the nitrogen cycle across spatial scales:
642 potentials, bottlenecks and solutions. *Earth-Sci. Rev.* 187, 248–258.

643 Zhu, Q., Schmidt, J.P., Bryant, R., 2012. Hot moments and hot spots of nutrient losses from a mixed land use watershed. *J.*
644 *Hydrol. Eng.* 414, 393–404.

645 Zhuang, Q., Romanovsk, V., McGuire, A., 2001. Incorporation of a permafrost model into a large-scale ecosystem model:
646 Evaluation of temporal and spatial scaling issues in simulating soil thermal dynamics. *J. Geophys. Res.* 106, 33649–
647 33670.

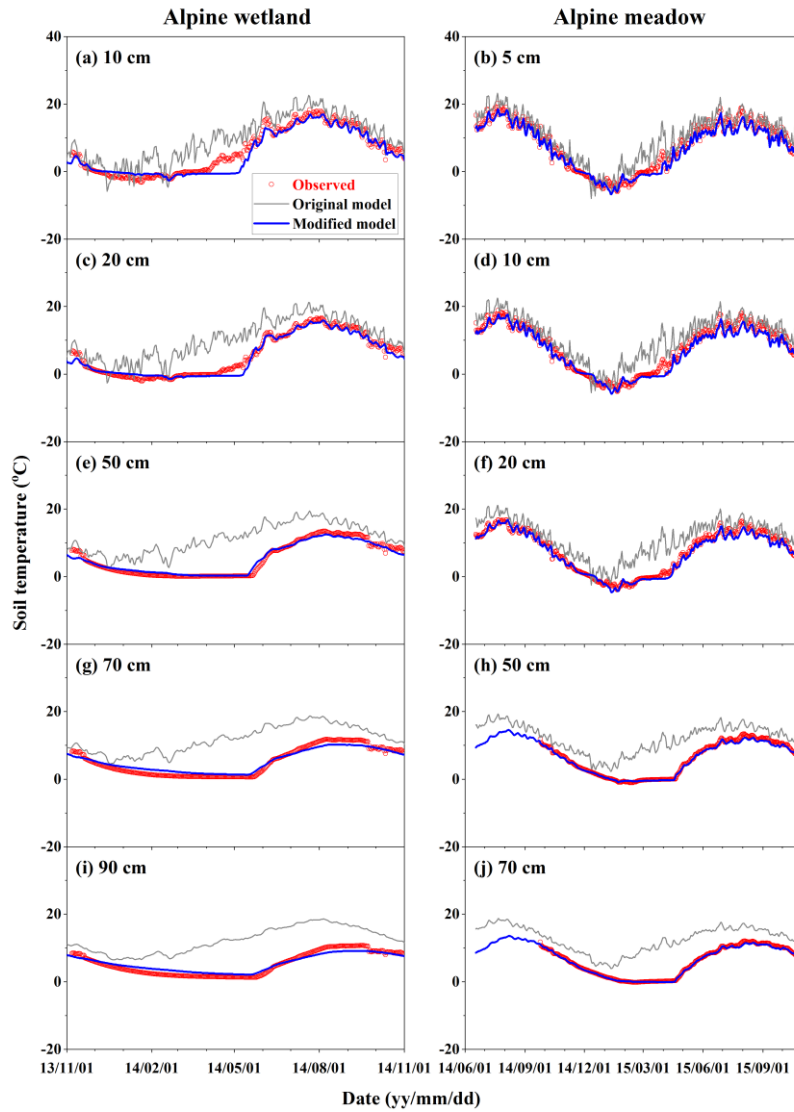
648 Zhuang, Q., Melillo, J., Kicklighter, D., Prinn, R., McGuire, A., Steudler, P., Felzer, B., Hu, S., 2004. Methane fluxes
649 between terrestrial ecosystems and the atmosphere at northern high latitudes during the past century: a retrospective
650 analysis with a process-based biogeochemistry model. *Glob. Biogeochem. Cycl.* 18, GB3010,
651 doi:10.1029/2004GB002239.

652
653
654

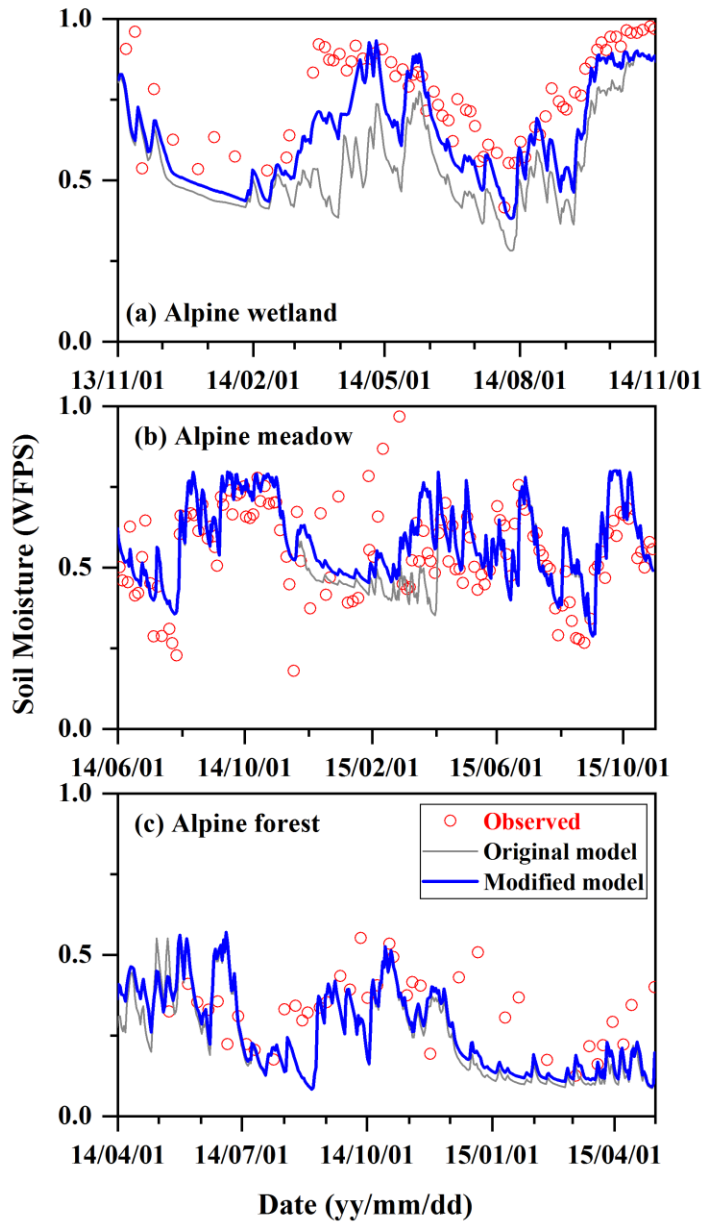
Table 1 Statistics of the validated variables by the modified CNMM-DNDC for three typical alpine ecosystems.

Item	Ecosystem	n^a	DR ^b	IA		NSE		ZIR-slope		ZIR- R^{2c}		ZIR-P	
				O ^c	M ^d	O	M	O	M	O	M	O	M
Soil temperature													
5 cm	Meadow	500	Daily	0.90	0.96	0.82	0.95	0.84	1.09	0.89	0.96	< 0.001	< 0.001
	Forest	48	Daily	0.85	0.91	0.37	0.68	0.64	0.83	0.68	0.73	< 0.001	< 0.001
10 cm	Wetland	366	Daily	0.90	0.98	0.57	0.92	0.72	1.07	0.81	0.93	< 0.001	< 0.001
	Meadow	500	Daily	0.93	0.99	0.71	0.95	0.80	1.08	0.85	0.96	< 0.001	< 0.001
20 cm	Wetland	366	Daily	0.82	0.99	0.18	0.96	0.64	1.05	0.66	0.97	< 0.001	< 0.001
	Meadow	500	Daily	0.87	0.99	0.48	0.97	0.74	1.06	0.76	0.98	< 0.001	< 0.001
50 cm	Wetland	366	Daily	0.66	0.99	-1.01	0.97	0.51	1.05	0.43	0.97	< 0.001	< 0.001
	Meadow	401	Daily	0.70	1.00	-0.48	0.99	0.58	1.06	0.53	1.00	< 0.001	< 0.001
70 cm	Wetland	366	Daily	0.58	0.98	-2.23	0.93	0.47	1.05	0.38	0.93	< 0.001	< 0.001
	Meadow	401	Daily	0.64	1.00	-1.19	0.99	0.54	1.03	0.49	1.00	< 0.001	< 0.001
90 cm	Wetland	366	Daily	0.52	0.98	-4.07	0.90	0.44	1.03	0.36	0.90	< 0.001	< 0.001
Soil moisture	Wetland	74	Daily	0.63	0.83	-1.65	0.20	1.31	1.13	–	0.60	–	< 0.001
	Meadow	128	Daily	0.78	0.78	0.28	0.32	0.96	0.93	0.30	0.41	< 0.001	< 0.001
	Forest	40	Daily	0.48	0.49	-1.04	-0.80	1.21	1.19	–	–	–	–
Daily CH ₄ flux	Wetland	180	Daily	0.37	0.74	-11.1	-0.73	0.46	0.87	–	–	–	–
	Meadow	168	Daily	0.87	0.88	0.42	0.38	1.09	0.94	0.44	0.39	< 0.001	< 0.001
	Forest	49	Daily	0.59	0.57	-2.79	-3.39	0.92	0.79	–	–	–	–
Daily N ₂ O flux	Wetland	180	Daily	0.01	0.26	-323	-0.07	0.01	0.59	–	–	–	–
	Meadow	168	Daily	0.23	0.44	-0.16	-1.76	0.99	0.35	–	–	–	–
	Forest	58	Daily	0.47	0.47	-1.85	-1.64	0.44	0.47	–	–	–	–

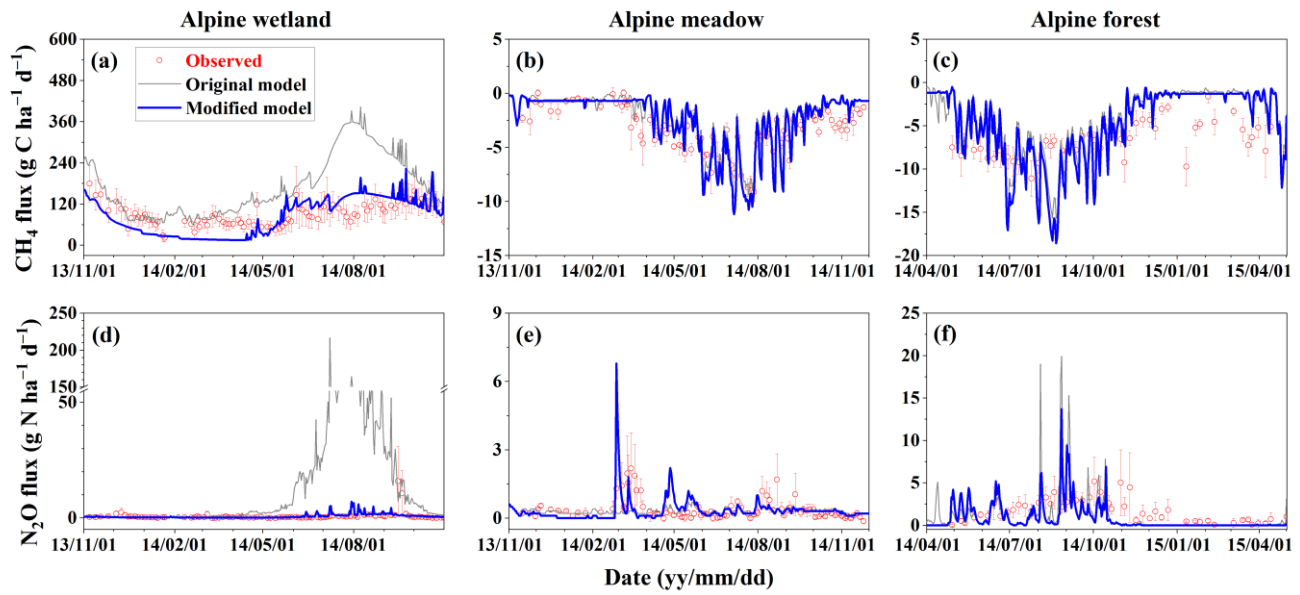
655 ^a n indicates the number of the observations. ^b DR denotes the time resolution of the observed data. ^c O indicates the simulations by the original
656 model. ^d M indicates the simulations by the modified model. ^e “–” indicated no value due to the sum of regression square are larger than the sum
657 of the total square for the regression). IA, NSE, ZIR-slope, ZIR- R^2 and ZIR-P indicate the index of agreement, Nash–Sutcliffe efficiency,
658 determination coefficient and slope of the zero-intercept univariate linear regression (ZIR) of the observations against the simulations, as well as
659 the significance level of the ZIR.



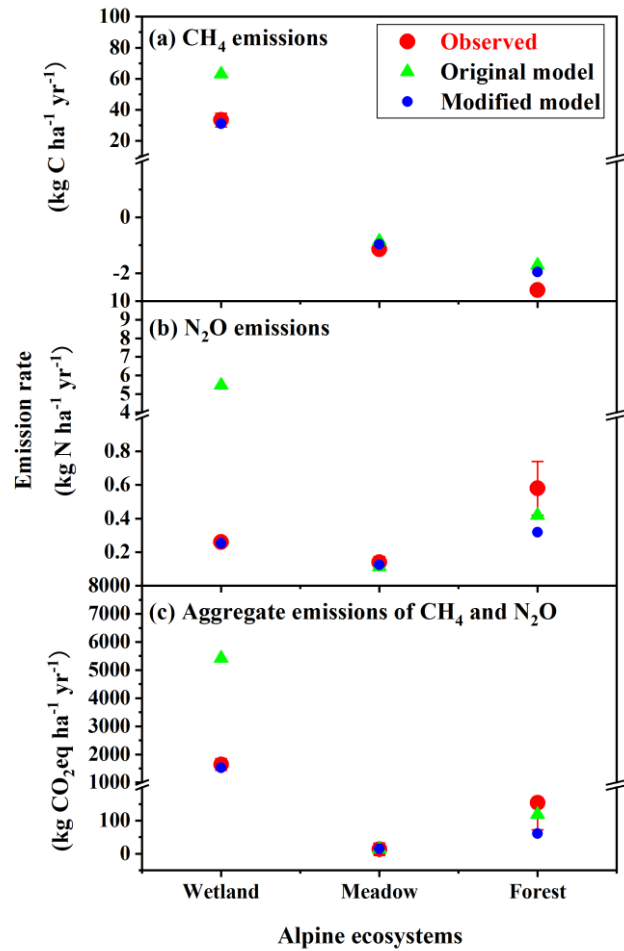
660
 661 **Figure: 1** Observed and simulated daily profile soil temperature from the alpine wetlands and meadows by the original and
 662 **modified models. The legends in panel a apply for all panels.**



663
 664 **Figure: 2** Observed and simulated daily topsoil (0–6 cm) moisture in the water-filled pore space (WFPS) from the alpine wetlands,
 665 meadows and forests by the original and modified models. The legends in panel a apply for all panels.



666
 667 **Figure: 3 Observed and simulated daily methane (CH₄) and nitrous oxide (N₂O) fluxes from the alpine wetlands, meadows and**
 668 **forests by the original and modified models. The vertical bar for each observation indicates the standard error of six spatial**
 669 **replicates. The legends in panel a apply for all panels.**



670

671 **Figure: 4** Observed and simulated annual emissions of methane (CH₄), nitrous oxide (N₂O) and aggregate emissions of both from
 672 the alpine wetlands (Wetland), meadows (Meadow) and forests (Forest). The legends in panel a apply for all panels.